Flexible Launch Vehicle Stability Analysis Using Steady Rigid CFD with Unsteady Aerodynamic Corrections

Robert E. Bartels*
NASA Langley Research Center, Hampton, VA, 23681, USA

This paper will present a method of correcting a quasi-static aeroelastic stability analysis of a launch vehicle. A quasi-static aeroelastic stability analysis is often unconservative at the critical Mach number where experiment or unsteady computational aeroelastic (CAE) analysis shows a reduced or even negative modal damping. Often a reduced stability margin is found in the transonic range. The corrections use unsteady computational fluid dynamics (CFD) based on the response of a modal excitation. The Fourier transform of the excitation response provides the correction. The quasi-static problem is formulated in complex state space. The eigenvalues of the corrected quasi-static analysis are compared with the damping and frequency computed using unsteady CAE analysis. The results show that this method of correction brings the quasi-static aeroelastic into close agreement with the unsteady CAE analysis.

Nomenclature

B_{cfd}	Projection matrix, structure to CFD surface nodes
B_{ll}	Projection matrix, structure to section loads analysis points
$\hat{c}$	X,Y,Z non-dimensional force coefficients per unit vehicle length
$\mathbf{F}$	Flow variable flux vector
$\mathbf{F}^*$	Flux vector for moving volume
g	Generalized variable
G	Generalized force vector
q_∞	Free stream dynamic pressure
S	Reference area
T_y	Y transformation matrix
T_z	Z transformation matrix
U_∞	Free stream velocity
$\mathbf{W}$	Velocity of control volume surfaces
α	Angle of attack
β	Angle of side slip
$\vec{\Delta}$	Total displacement vector
$\vec{\delta}_0$	Rigid body displacement vector
$\vec{\delta}_s$	Static aeroelastic displacement vector
$\vec{\delta}_d$	Dynamic aeroelastic displacement vector
Δ	Structural and aerodynamic damping matrix
ϕ	Matrix of eigenvectors of structural dynamic equations
Φ_{cfd}	Modal vectors projected to the CFD surface mesh
Φ_{ll}	Modal vectors projected to the section loads analysis points
χ	State variable vector
ζ_s	Structural damping ratio
ζ_{ss}	Static structural damping ratio
ζ_{sd}	Dynamic structural damping ratio
ζ_a	Aerodynamic damping ratio
ζ	Total damping ratio
ω	Modal frequency of vehicle structure
Ω	Structural and aerodynamic stiffness matrix

*Aerospace Engineer, Aeroelasticity Branch, Senior Member

Subscript
l Local
ll Lineloads
s Static
d Dynamic

Note to Reviewer: The predicted performance and certain other features and characteristics of the Ares I and Ares I-X launch vehicles are defined by the U.S. Government to be Sensitive but Unclassfied (SBU). Therefore, details have been removed from all plots and figures and tabulated data may have been rescaled.

I. Introduction

The Vision for Space Exploration and the NASA Authorization Act of 2005 directed NASA to develop the technology to open the space frontier, to send astronauts back to the Moon and possibly to Mars as well. The Constellation program is tasked with developing the tools necessary to execute these next steps in the U.S space exploration program. Within that program the Ares and the Orion programs develop the crew launch vehicle (CLV) and crew capsule technology. The Ares program has the task of developing the vehicle necessary to launch the crew capsule and associated hardware to provide transport to destinations beyond low earth orbit.

The engineering of the Ares CLV is a departure from the past development of launch vehicles in that CFD will be an integral part of the design from the conceptual stage. The vehicle will be designed with the smallest ever proportion of aerodynamic data derived from wind tunnel testing and the largest ever component due to computational fluid dynamics. This poses both exciting possibilities in the extent to which the aerodynamics and flow field physics of a launch vehicle can be understood as well as challenges in validating methodologies for the highly complex flow field about a launch vehicle.

Aeroelastic stability has been a concern since early development of the Saturn I.[1,2] Vehicles with a hammerhead configuration, having a larger diameter upper stage, have the potential for aeroelastic instability.[3,4] One of the notable features of the Ares CLV is the use of a five segment Solid Rocket Booster (SRB) as a first stage with a larger diameter upper stage. The two stages are connected by an aft facing inter-stage frustum. Along with the usual geometric complexity of protuberances over a major launch vehicle, this hammer-head configuration poses a challenge to CFD analysis because it has the potential of producing flow field separation from the frustum. Combined with shock separation over the upper stage, this frustum separation can significantly influence overall vehicle aerodynamics.[4,3,5] The extent of separated flow over the Ares vehicle has motivated the wide spread use of high fidelity Navier-Stokes analyses. This includes modeling fluid/structure interaction with a high fidelity Navier-Stokes flow solver coupled with a model of the structural dynamics.

The potential for coupling shock dynamics and shock separation over a conical fore-body and a boat tail flow separation is well known. The SRB aft skirt adds an additional mechanism for dynamic aeroelastic instability due to the disturbance time lag between the upper stage, inter-stage frustum and the aft skirt.[4] Ericsson has developed a quasi steady analytical method of sectional loads using steady state wind tunnel data that incorporates corrections to the aerodynamic damping based on a disturbance time lag between the fore and aft body regions. This lag is due to the time required for boundary layer separation to grow in response to vehicle motion in an unsteady flow compared to a steady flow field. Furthermore, convection times add an additional time lag. The analytical/empirical approach of Ericsson does provide an initial rapid and possibly conservative approximation to the phase shift,[3] and the destabilizing effect of unsteady aerodynamics.

A comparison of aeroelastic stability analyses using quasi-steady section loading and computational aeroelastic analysis using the unsteady unstructured Reynolds averaged FUN3D code of the flexible Ares 1 has been shown.[6] The unsteady FUN3D aeroelastic analysis at Mach 1 showed the aerodynamics of mode one to be significantly undamped. The flexiblized/rigid integrated line loads (FRILLS) method proved to be unconservative at the critical Mach 1 condition. The first mode aerodynamic damping derived from the quasi-static FRILLS method was significantly positive.

The present paper provides a dynamic correction to the FRILLS method that allows a much more accurate modeling of the magnitude change and phase shift of the sectional loading due to unsteady aerodynamics. This work presents a modernization of the method of Ericsson and Redding. Their method used empirical formulations to estimate the phase shift due to unsteady shock motion and flow field separation. The present method uses CFD and Fourier analysis of section loads to account for the effect of unsteady aerodynamics.

II. Methods of Analysis

A. FUN3D Aeroelastic Solver

The Navier-Stokes code used in this study is FUN3D. The Fully Unstructured Navier-Stokes Three-Dimensional (FUN3D) flow solver is a finite-volume unstructured CFD code for either compressible or incompressible flows.[7,8] Flow variables are stored at the vertices of the mesh. FUN3D can solve the discrete compressible Euler or Reynolds-averaged Navier-Stokes (RANS) flow equations either tightly or loosely coupled with a turbulence model on mixed element grids, including tetrahedral, prisms and hexahedra. In the present study the RANS solver and the loosely coupled Spalart-Allmaras turbulence model are used on an all tetrahedron grid.[9] FUN3D employs an implicit upwind algorithm in which the inviscid fluxes are obtained with a flux-splitting scheme. At interfaces delimiting neighboring control volumes, the inviscid fluxes are computed using an approximate Riemann solver based on the values on either side of the interface. Interface values are obtained by a least squares extrapolation using gradients computed at the vertices. Reconstruction requires limiting for flows with shocks. A variety of gradient limiters are available. In the present study the low dissipation flux splitting scheme for the inviscid flux construction, and the blended Van Leer flux limiter[10] were used. For tetrahedral meshes the full viscous fluxes are made discrete by using a finite-volume formulation in which the required velocity gradients on the dual faces are computed using the Green-Gauss theorem.[11] This is equivalent to a Galerkin type approximation. The solution at each time step is updated with a backwards Euler time differencing scheme and the use of local time stepping. At each time step, the linear system of equations is approximately solved either with a multi-color point-implicit procedure or an implicit-line relaxation scheme.[12] Domain decomposition exploits the distributed high-performance computing architectures that are necessary for the grid sizes used in the present study.

For a moving mesh, the conservation equations are written in the Arbitrary Lagrange Euler (ALE) formulation.[13] The unsteady Navier-Stokes equations written in integral form for a moving control volume are

$$\frac{\partial}{\partial t}\int_V \mathbf{q}\,dV + \int_{\partial V}(\mathbf{F}^* - \mathbf{F}_v)\cdot\hat{\mathbf{n}}\,dS = 0 \tag{1}$$

For a moving mesh the flux through the control volume is $\mathbf{F}^* = \mathbf{F} - \mathbf{q}\mathbf{W}^T$ where $\mathbf{F}$ is the flow variable flux vector associated with a stationary control volume. The vector $\mathbf{q}$ is the vector of conserved variables and the vector $\mathbf{W}$ represents the velocity of the local control volume surfaces. Additional information on the FUN3D implementation of the ALE formulation is found in reference[13].

The mesh deformation is accomplished by treating the mesh motion as analogous to a linear elasticity problem.[14] The linear elasticity equations written in differential form are

$$\nabla\cdot\sigma = 0 \tag{2}$$

where the stress tensor is given by $\sigma = \lambda Tr(\varepsilon)\mathbf{I} + 2\mu\varepsilon$ where Tr is the trace, $\mathbf{I}$ is the identity tensor, λ and μ are material properties and ε is the strain tensor. By use of the Gauss divergence theorem the elasticity equations can be written in finite-volume form and evaluated in a manner similar to the integration of the conservation form of the flow equations. The material properties vary based on distance to the nearest solid boundary. In contrast to the original implementation[14] in which the Poisson ratio is varied, elements near a solid boundary are made significantly stiffer by specifying the value of E, the Youngs modulus. The Poisson ratio ν is given a uniform value of zero. The displacements are computed from the finite volume formulation of the elasticity equations using the GMRES algorithm.[13,15]

In the present aeroelastic analysis FUN3D utilizes a modal decomposition of the structural model. This method has been validated for the FUN3D code elsewhere against the AGARD 445.6 wing flutter onset wind tunnel data.[13] An orthogonal transformation of the finite element equations provides the eigenvalues and eigenvectors from which the mode shapes and structural frequencies are derived. The transformed equations of structural dynamics are

$$[I]\{\ddot{g}\} + [2\zeta_s\omega]\{\dot{g}\} + \left[\omega^2\right]\{g\} = q_\infty[\phi]^T\{f\} \tag{3}$$

The eigenvectors of the modal transformation are projected on to the CFD surface node points.

$$\left[\Phi_{cfd}\right] = \left[B_{cfd}\right][\phi] \tag{4}$$

where $\left[B_{cfd}\right]$ is an $N_{st}\times 3N_{cfd}$ projection matrix relating structural centerline nodes to CFD surface nodes, $[\phi]$ is a $N_{modes}\times N_{st}$ matrix of eigenvectors and , $\left[\Phi_{cfd}\right]$ is a $N_{modes}\times 3N_{cfd}$ matrix of mode shapes projected to the CFD surface nodes.

B. Dynamic Aeroelastic Analysis Based on Section Loads Including Dynamic Correction

A review of the method of section loads for launch vehicles is presented in a paper by Bartels.[6] The present paper provides a method to incorporate dynamic magnitude and phase corrections to the flexiblized rigid integrated line loads (FRILLS) method.

The essence of this method is to simplify the aeroelastic response of the vehicle to displacements along the vehicle axis and apply elastic, inertial and aerodynamic forces distributed discretely along the vehicle axis. The vehicle is partitioned into N_{ll} stations along the vehicle axis. Displacements at each station can be written as a sum of rigid body displacements, static aeroelastic and dynamic aeroelastic displacements. The displacement is defined $\vec{\Delta} = (\Delta_{1x}, \Delta_{1y}, \Delta_{1z}, \cdots, \Delta_{N_{ll}x}, \Delta_{N_{ll}y}, \Delta_{N_{ll}z})^T$ at N_{ll} stations, where

$$\vec{\Delta} = \vec{\delta}_0 + \vec{\delta}_s + \vec{\delta}_d \quad , \quad \vec{\delta}_s = f(x) \quad , \quad \vec{\delta}_d = f(x,t) \tag{5}$$

where δ_0 is a rigid vehicle centerline displacement vector and δ_{zs} and δ_{zd} are the static and dynamic aeroelastic centerline displacements, respectively. The material derivative yields and approximation for the local angles of attack and side slip

$$\{\alpha_l\} \approx \alpha + \frac{1}{U_\infty}[T_z]\{\frac{\partial \vec{\delta}_d}{\partial t} + \left(\frac{\partial \vec{\delta}_s}{\partial x} + \frac{\partial \vec{\delta}_d}{\partial x}\right)\} \quad , \quad \{\beta_l\} \approx \beta + \frac{1}{U_\infty}[T_y]\{\frac{\partial \vec{\delta}_d}{\partial t} + \left(\frac{\partial \vec{\delta}_s}{\partial x} + \frac{\partial \vec{\delta}_d}{\partial x}\right)\} \tag{6}$$

where matrices $[T_y]$ and $[T_z]$ are defined in the Appendix.

Modal analysis of the finite element model provides mode shapes that are projected to these same points along the vehicle. The projection can be written

$$[\Phi_{ll}] = [B_{ll}][\phi] \tag{7}$$

where $[B_{ll}]$ is an $3N_{st} \times 3N_{ll}$ projection matrix relating structural and sectional loads analysis centerline nodes, and $[\Phi_{ll}]$ is a $N_{modes} \times 3N_{ll}$ matrix of mode shapes projected to the sectional loads analysis centerline nodes. The matrices $[B_{ll}]$ and $[B_{cfd}]$ use the same method of projection to ensure consistency of the sectional loads results and the FUN3D CAE results. The modal transformation yields

$$g = g_s + g_d = [\phi]^T [B_{ll}]^T \left(\vec{\delta}_s + \vec{\delta}_d\right) \tag{8}$$

Where g_s is the generalized variable due to static loading and g_d is the generalized variable responding to vehicle dynamics. The generalized forcing due to aerodynamics can be written in terms of the $3 \times N_{ll}$ dimensional section loading $\hat{c}$

$$G = \frac{q_\infty S \Delta x}{Dia}[\phi]^T [B_{ll}]^T \hat{c} \tag{9}$$

where

$$\hat{c} = (\hat{c}_{1x} \quad \hat{c}_{1y} \quad \hat{c}_{1z} \quad \cdots \quad \hat{c}_{N_{ll}x} \quad \hat{c}_{N_{ll}y} \quad \hat{c}_{N_{ll}z})^T \tag{10}$$

The aerodynamic loading at each body station n, $\hat{c}_{nx}$, $\hat{c}_{ny}$, $\hat{c}_{nz}$ are functions of Mach number, angle of attack and angle of side slip.

The sectional aerodynamics is computed by integrating nondimensional pressure coefficients from the vehicle surface using the FUN3D (or any CFD method such as USM3D) solution.[16] The integration is accomplished using a discrete data transfer algorithm based on a method of Farhat, Lesoinne and LeTallec,[17] which is a variation of the inverse isoparametric method (IIM). The further modified IIM algorithm of Samareh[16] maintains conservation of momentum and energy between separate meshes having dissimilar mesh spacing by an integration of loads on the source mesh and injection of the force vectors to the target mesh. Having transferred discrete loads from the unstructured CFD mesh to the sectional mesh, the nodal loads are integrated into sectional loads. A data base of sectional loads is assembled by computing CFD solutions for the rigid vehicle at each Mach number at a series of angles of attack. Aerodynamic section loading along the vehicle body from this series of solutions is input to the present analysis. To facilitate the following analysis, $N_{ll} \times N_{ll}$ square matrices $[\hat{c}]$, $\partial[\hat{c}]/\partial\alpha$ and $\partial[\hat{c}]/\partial\beta$ are constructed placing along the diagonals the values of $\hat{c}$ or its derivatives. The derivatives are computed from a spline fit of the aerodynamic section loadings as functions of angle of attack and sideslip.

The static aeroelastic solution method is discussed elsewhere.[6] The dynamic response of the vehicle can be computed by linearizing the line loads around the local static α_l, β_l and static generalized force G_s. This can be written

$$[I]\{\ddot{g_d}\} + \left[[2\zeta_{sd}\omega] - \tilde{N}\right]\{\dot{g_d}\} + \left[\left[\omega^2\right] - \tilde{N}'\right]\{g_d\} = G_s \tag{11}$$

where $\tilde{N} = N_r + iN_i$, $\tilde{N}' = N'_r + iN'_i$ and

$$N_r = q_\infty S \frac{\Delta x}{U_\infty} [\phi]^T [B_{ll}]^T \left\{ \frac{\partial [\hat{c}]}{\partial \alpha}|_r [\hat{S}] [T_z] + \frac{\partial [\hat{c}]}{\partial \beta}|_r [\hat{S}] [T_y] \right\} [B_{ll}] [\phi] \tag{12}$$

$$N_i = q_\infty S \frac{\Delta x}{U_\infty} [\phi]^T [B_{ll}]^T \left\{ \frac{\partial [\hat{c}]}{\partial \alpha}|_i [\hat{S}] [T_z] + \frac{\partial [\hat{c}]}{\partial \beta}|_i [\hat{S}] [T_y] \right\} [B_{ll}] [\phi] \tag{13}$$

and

$$N'_r = q_\infty S \Delta x [\phi]^T [B_{ll}]^T \left\{ \frac{\partial [\hat{c}]}{\partial \alpha}|_r [\hat{S}] [T_z] + \frac{\partial [\hat{c}]}{\partial \beta}|_r [\hat{S}] [T_y] \right\} [B_{ll}] \left[\frac{\partial \phi}{\partial x} \right] \tag{14}$$

$$N'_i = q_\infty S \Delta x [\phi]^T [B_{ll}]^T \left\{ \frac{\partial [\hat{c}]}{\partial \alpha}|_i [\hat{S}] [T_z] + \frac{\partial [\hat{c}]}{\partial \beta}|_i [\hat{S}] [T_y] \right\} [B_{ll}] \left[\frac{\partial \phi}{\partial x} \right] \tag{15}$$

and G_s represents the converged static aeroelastic aerodynamic loading at $\alpha_l(x)$ and $\beta_l(x)$. The notation $()|_r$ and $()|_i$ represents the real and imaginary parts of the section loads. The complex value is obtained from the Fourier phase/magnitude of the unsteady section aerodynamics. The first and second modes are oscillated separately using the unsteady aeroelastic FUN3D code to obtain a time history of the loads at each body section. The first and second modes are oscillated using the FRILLS method to obtain a time history of the loads at each body section. The corrected line loads are derived from

$$\hat{c}|_r = Re \left[\hat{c} R e^{i\Delta\psi} \right] \tag{16}$$

$$\hat{c}|_i = Im \left[\hat{c} R e^{i\Delta\psi} \right] \tag{17}$$

$$R = \frac{mag(\bar{c}_d)}{mag(\bar{c}_s)} \qquad , \qquad \Delta\psi = phase(\bar{c}_d) - phase(\bar{c}_s) \tag{18}$$

The parameter $\bar{c}_s$ is the Fourier transform of the FRILLS quasi-static section load time history and $\bar{c}_d$ is the Fourier transform of the unsteady aerodynamic section load time history. The term $\Delta\psi$ is the difference between the phase of the unsteady and quasi-static solutions. These values are determined at each section along the vehicle.

Equation 11 can be written in state space

$$\dot{\chi} = [A] \chi + \{\chi\}_s \tag{19}$$

where

$$[A] = [A_r] + i [A_i] \tag{20}$$

$$[A_r] = \begin{bmatrix} 0 & I \\ -\Omega_r & -\Delta_r \end{bmatrix} \tag{21}$$

$$[A_i] = \begin{bmatrix} 0 & I \\ -\Omega_i & -\Delta_i \end{bmatrix} \tag{22}$$

and

$$\{\chi\}_s = \begin{bmatrix} 0 \\ G_s \end{bmatrix} \tag{23}$$

The complex frequency and damping matrices are

$$\Omega_r = \omega^2 - N_r \qquad , \qquad \Omega_i = \omega^2 - N_i \tag{24}$$

$$\Delta_r = 2\zeta_{sd}\omega - N'_r \qquad , \qquad \Delta_i = 2\zeta_{sd}\omega - N'_i \tag{25}$$

The complex eigenvalues of the complex matrix A provide aeroelastic damping and frequency at a given flight condition.

III. Models

A. CFD Mesh

The unstructured tetrahedral mesh is created using VGRID.[18] Before performing the CAE analysis a study of the acceptable level of grid convergence was performed. In the pursuit of this strategy, four grids were developed (See Figures 2-10), designated the extra coarse, coarse, baseline and fine grids. The extra coarse grid had 10 million nodes, the coarse grid had 19 million nodes, the baseline had 41 million nodes and the fine grid had 83 million nodes. The refinement of successive grid levels was accomplished by doubling the number of surface nodes, and otherwise keeping the boundary layer spacing normal to the vehicle surface unchanged. All clustered and non-clustered areas were refined uniformly. Grid convergence is discussed in detail in a separate paper.[19]

B. Structure Model

The structural models used in the Ares I-X and Ares 1 analyses are $MSC.Nastran^{TM}$ finite element models. The Ares I-X model is designated Integrated Vehicle Model 12 (IVM12). Two Ares 1 models were used in the present analysis. The baseline Ares 1 model is designated Ares Integrated Model 1 (LC4-AIM1). The second Ares 1 model is otherwise identical but includes a upper stage Thrust Oscillation Isolator (TOI). The Ares I-X model includes a finite element modeling of the first stage, first stage solid propellant, second stage mass simulator, the Crew Exploration Vehicle (CEV) simulator and the Launch Abort System (LAS) simulator. The Ares 1 model includes a finite element modeling of the first stage, first stage solid propellant, second stage including liquid fuel and oxidizer masses, the CEV and LAS.

The Orion configuration utilized in the present Ares 1 analysis is the liftoff configuration for the lunar mission. The Orion structural data consists of a stiffness matrix produced by Craig-Bampton analysis, retaining information only along the centerline and an interface circumference where the Orion connects to the upper stage. The upper stage configuration contains fluid elements, pressure stiffening, and temperature effects associated with the Wetchill state of the J-2X. The first stage solid propellant is modeled as four concentrated masses. Because the first stage propellant mass changes during atmospheric ascent there is a continuous change in the stiffness and mass properties of the first stage. First stage propellant mass data was defined at a rather coarse spacing of ascent times, namely at T0, 20, 40, 50 60, 80, 100 to 115 seconds. The lunar mission trajectory data, including total vehicle mass is defined significantly more finely. To apply propellant mass data in a consistent manner the coarsely spaced propellant data was interpolated to the present analysis points by matching total mass with the trajectory vehicle mass.

An additional Ares 1 structural model is used in the present analysis that incorporates a Thrust Oscillation Isolator (TOI). The TOI is a dual plane isolation system intended to isolate the upper stage from second stage thrust oscillation. The isolator mechanism was modeled by a circumferential ring of springs at the interface between the Orion and the upper stage, and a circumferential ring of spring elements and mass elements at the interface between the upper stage and the first stage. In all other respects the TOI model is identical to the baseline Ares 1 structural model.

The entire Ares 1 vehicle structural model was reduced to 51 points along the vehicle centerline by a Guyan reduction and translational and rotational modal deflections were obtained. Mode shapes having only axial or rotational deflections were discarded for the present analysis. The remaining modes were ranked by the moduli of the mode shape amplitude and the top 44 flexible modes for the Ares I-X and 37 flexible modes for the Ares 1 were retained. The translational deflections of the remaining modes were projected with a spline fit to the CFD surface mesh points.

Thirty seven modes have been retained in the aeroelastic analysis of the Ares 1. The first two are vehicle bending modes that are orthogonal to each other. The first mode is the one that shows the least stability in the transonic range. The structural damping ratio used in the present analysis is 0.005.

IV. Dynamic Aeroelastic Results

Dynamic aeroelastic analyses have been performed to assess the aeroelastic stability of the Ares I vehicle. The ascent condition at Mach 1 $\alpha = 0$ degrees has been shown to be the least stable.[6] A computational aeroelastic solution using the TOI model with a structural damping ratio of 0.005 is marginally stable in the first mode at nominal dynamic pressure. The yellow triangle symbols in the following figures present this solution. These results represent the standard against which the corrected FRILLS results are compared.

In order to obtain the aerodynamic corrections for this condition, solutions were obtained with FUN3D and FRILLS in which mode 1 and 2 of the TOI structural model were given an oscillatory excitation. The section load response to the oscillation of each of those modes was processed using a discrete fast Fourier transform. Figure 1 shows the magnitude and phase of the Fourier transform of the unsteady FUN3D and quasi-static FRILLS time histories.

The FRILLS method with and without an aerodynamic correction has been computed. Results are shown in

Figure 2. These results show that the correction based on unsteady aerodynamics significantly improves the stability prediction of the quasi-static aeroelastic analysis. The final paper will show additional results as well as a study of time step sensitivity of the excitation/response.

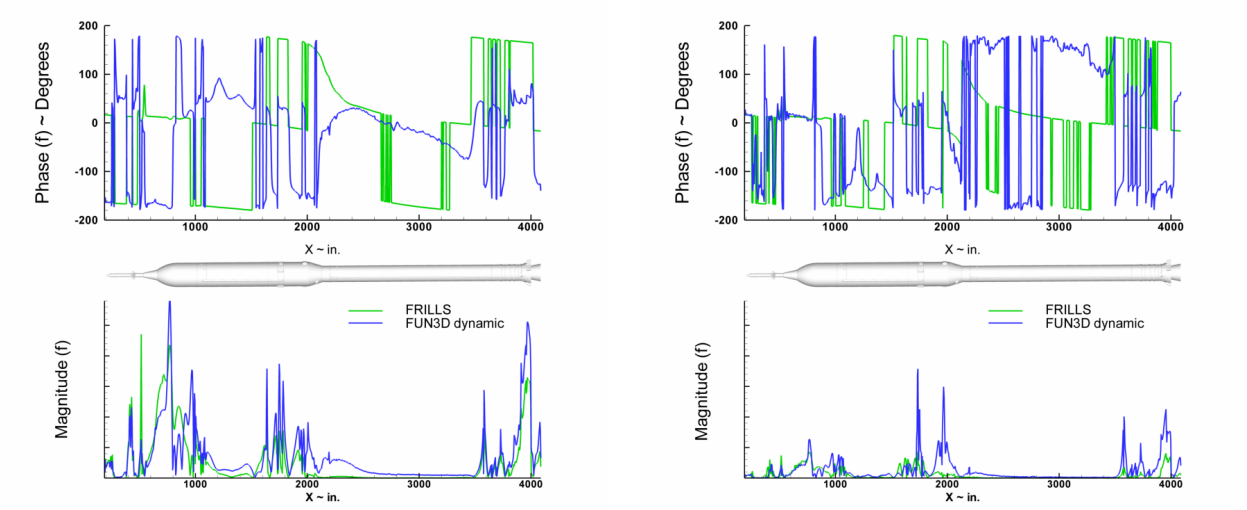

(a) Mode 1 (b) Mode 2

Figure 1. Phase and Magnitude of Section Loads

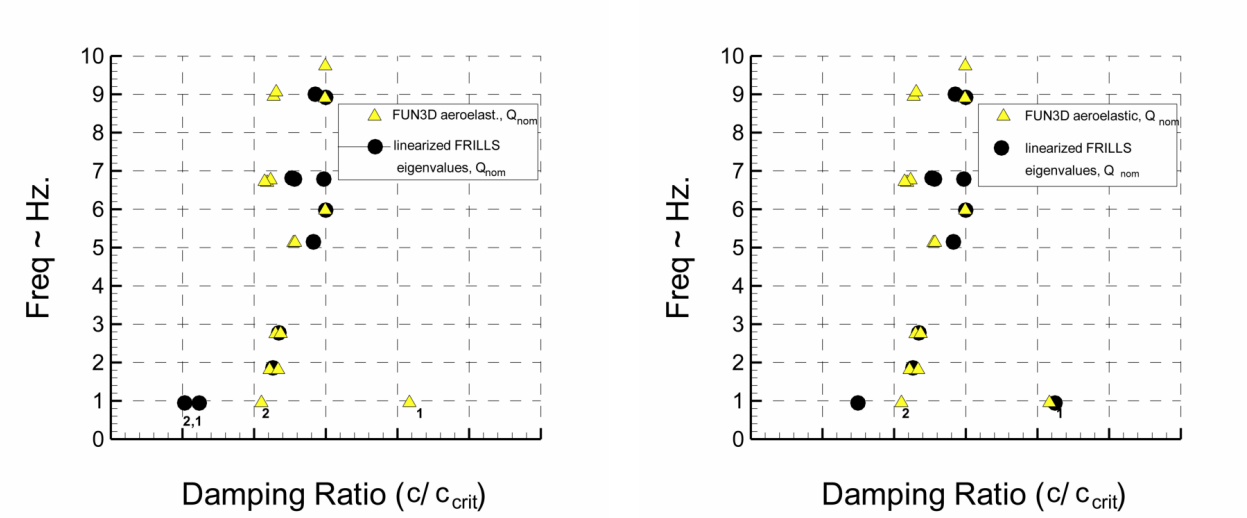

(a) Without Correction (b) With Correction

Figure 2. Frequency versus Damping

References

[1]Hanson, P. W. and Doggett, R. V. J., "Aerodynamic Damping and Buffet Response of an Aeroelastic Model of the Saturn I Block II Launch Vehicle," NASA Technical Note NASA TN D-2713, 1965.

[2]Dogget, R. V. J. and W., H. P., "An Aeroelastic Model Approach for the Prediction of Buffet Bending Loads on Launch Vehicles," NASA Technical Note NASA TN D-2022, 1963.

[3]Ericsson, L. E. and Pavish, D., "Aeroelastic Vehicle Dynamics of a Proposed Delta II 7920-10L Launch Vehicle," *Journal of Spacecraft and Rockets*, Vol. 37, No. 1, 2000, pp. 28–38.

[4]Ericsson, L. E., "Aeroelastic Instability Caused by Slender Payloads," *Journal of Spacecraft*, Vol. 4, No. 1, 1967, pp. 65–73.

[5]Ericsson, L. E., "Unsteady Flow Separation Can Endanger the Structural Integrity of Aerospace Launch Vehicles," *Journal of Spacecraft and Rockets*, Vol. 38, No. 2, 2001, pp. 168–179.

[6]Bartels, R., Chwalowski, P., Massey, S., Heeg, J., Wieseman, C., and Mineck, R., "Computational Aeroelastic Analysis of the Ares Launch Vehicle During Ascent," *28th AIAA Applied Aerodynamics Conference*, No. 4374, 2010.

[7]Anderson, W. K., Rausch, R. D., and Bonhaus, D. L., "An Implicit Upwind Algorithm for Computing Turbulent Flows on Unstructured Grids," *Computers and Fluids*, Vol. 23, No. 1, 1994, pp. 1–22.

[8]NASA LaRC, Hampton, VA, *FUN3D Manual*, Nov. 2008, http://fun3d.larc.nasa.gov.

[9]Spalart, P. R. and Allmaras, S. R., "One-Equation Turbulence Model for Aerodynamic Flows," *30th AIAA Aerospace Sciences Meeting and Exhibit*, No. 439, 1992.

[10]Vatsa, V. N. and White, J. A., "Calibration of a Unified Flux Limiter for Ares-Class Launch Vehicles from Subsonic to Supersonic Speeds," 56th Propulsion Meeting 5, JANNAF, III, April 2009.

[11]Rumsey, C. L. and Thomas, J. L., "Application of FUN3D and CFL3D to the Third Workshop on CFD Uncertainty Analysis," NASA Technical Memorandum NASA/TM-2008-215537, 2008.

[12]Nielsen, E. J., Lu, J., Park, M. A., and Darmofal, D. L., "An Exact Dual Adjoint Solution Method for Turbulent Flows on Unstructured Grids," *Computers and Fluids*, Vol. 33, No. 9, 2004, pp. 1131–1155.

[13]Biedron, R. T. and Thomas, J. L., "Recent Enhancements To The FUN3D Flow Solver For Moving-Mesh Applications," *47th AIAA Aerospace Sciences Meeting*, No. 1360, 2009.

[14]Nielsen, E. J. and Anderson, W. K., "Recent Improvements in Aerodynamic Design Optimiation on Unstructured Meshes," *AIAA Journal*, Vol. 40, No. 6, 2002, pp. 1155–1163.

[15]Saad, Y. and Schultz, M. H., "GMRES: A Generalized Minimum Residual Algorithm for Solving Nonsymmetric Linear Systems," *SIAM Journal of Scientific and Statistical Computing*, Vol. 7, 1986, pp. 856–869.

[16]Samareh, J. A., "Discrete Data Transfer Technique for Fluid-Structure Interaction," *18th AIAA Computational Fluid Dynamics Conference*, No. 4309, 2007.

[17]Farhat, C., Lesoinne, M., and LeTallec, P., "Load and Motion Transfer Algorithms for Fluid/Structure Interaction Problems with Non-Matching Discrete Interface: Momentum and Energy Conservation, Optimal Discretization and Application to Aeroelasticity," *Computer Methods and Applied Mechanical Engineering*, Vol. 157, No. 1, 1998, pp. 95–114.

[18]Pirzadeh, S. Z., "Advanced Unstructured Grid Generation for Complex Aerodynamic Applications," *26th AIAA Applied Aerodynamics Conference*, No. 7178, 2008.

[19]Bartels, R., Vatsa, V., Carlson, J.-R., Park, M., and Mineck, R., "FUN3D Grid Refinement and Adaptation Studies for the Ares Launch Vehicle," *28th AIAA Applied Aerodynamics Conference*, No. 4372, 2010.